Dual-Mode Switchable Liquid-Crystal Window

Yingfei Jiang, Yunho Shin, and Deng-Ke Yang*
Chemical Physics Interdisciplinary Program, Department of Physics and Advanced Materials and Liquid Crystal Institute, Kent State University, Kent, Ohio 44242, USA

(Received 13 May 2019; revised manuscript received 18 October 2019; published 15 November 2019)

Radiant energy-flow control and privacy control are two important features for smart windows (or glass). Current smart window technologies can, however, only control one of them: radiant energy flow or privacy. Therefore, a dual-mode smart window is highly desirable. Here, we report a dual-mode switchable liquid-crystal window that can control both radiant energy flow and privacy. The switchable liquid-crystal window makes use of dielectric and flexoelectric effects. In the absence of an applied voltage, the window is clear and transparent, and radiant energy can flow through it and the scenery behind the window can be seen. When a low-frequency (50 Hz) voltage is applied, the window is switched to an optical scattering and absorbing state by a flexoelectric effect, and thus, privacy is protected. When a high-frequency (1 kHz) voltage is applied, the window is switched to an optical absorbing but nonscattering state through a dielectric effect, and thus, radiant energy flow is controlled.

DOI: 10.1103/PhysRevApplied.12.054037

I. INTRODUCTION

Switchable smart windows (or glass) are important due to their applications in architecture, vehicles, eyeglasses, and various types of displays [1–5]. The functions of smart windows are radiant energy-flow control, privacy protection, or simply aesthetic. In radiant energy-flow control (visible- and near-infrared-light wavelength regions) applications, in one state, the window is transparent and allows radiant energy to flow through it; in another state, the window is absorbing (or reflecting) and reduces the radiant energy flow, but the scenery behind can be seen (the image is not distorted). By reducing radiant energy flow through windows, buildings and cars can be kept cooler on hot summer days. In privacy control (visible-light wavelength region) applications, in one state, the window is transparent and the scenery behind the window can be seen; in another state, the window is opaque (or frosted) and the scenery behind cannot be seen (the image is completely distorted), but radiant energy may still flow through. Notably, in radiant energy-flow control mode, if the transmittance is low enough, the window becomes black, and then it can also control privacy.

Depending on the active materials used, currently, smart window technologies can be categorized into three types: suspended particles [6], electrochromics [7–9], and liquid crystals [10]. Both suspended particle and electrochromic smart windows can only control radiant energy flow. Meanwhile, switching is slow, the contrast ratio may not be high, and the optical performance may be dependent on wavelength.

In the last couple of decades, liquid crystals (LCs) have been intensively studied for switchable smart windows. The competing technologies are polymer-dispersed liquid crystals (PDLCs), polymer-stabilized cholesteric textures (PSCTs), cholesteric liquid crystals, and dichroic dye-based guest-host liquid crystals. In a PDLC, nematic LC droplets are dispersed in an isotropic polymer [11–17]. When no voltage is applied, the orientation of the LC droplets is random and the effective refractive index of the LC droplets is not matched to that of the polymer; the material is scattering. When a voltage is applied, the LC droplets are aligned unidirectionally and the effective refractive index of the LC droplets matches that of the polymer; the material becomes transparent. In a PSCT, a small amount of polymer network is dispersed in a cholesteric LC [18–23]. When no voltage is applied, the LC is in a polydomain structure; the effective refractive index changes from one domain to another and the material is scattering. When a voltage is applied, the LC is unidirectionally aligned and forms a single domain, so the material becomes transparent. PDLCs and PSCTs can control privacy. A cholesteric liquid crystal possesses a periodic helical structure [24–30]. When no voltage is applied, the LC selectively reflects light in the wavelength region from $\lambda_1 = n_o P$ to $\lambda_2 = n_e P$, where P is the helical pitch of the LC and n_o and n_e are ordinary and extraordinary refractive indices, respectively, of the LC. When a sufficiently high voltage is applied, the helical structure is unwound and the material becomes transparent. For most cholesteric LCs, the reflection bandwidth is about 50 nm.

*dyang@kent.edu

To cover the visible- and near-infrared-light wavelength regions, a gradient of the helical pitch is required; this can be achieved by using polymer stabilization [31–34]. Therefore, cholesteric LCs can control radiant energy flow in visible- and near-infrared wavelength regions. Guest-host liquid crystals contain dichroic absorbing dyes, which are also elongated molecules [35–38]. When no voltage is applied, the LC and dye are parallel to the cell substrate, and thus, are parallel to the polarization of incident light; the materials are optically absorbing. When a voltage is applied, the LC and dye are aligned perpendicular to the cell substrate, and thus, perpendicular to the polarization of incident light; the material is transparent. For most dichroic dyes, the absorbing band can only cover the visible-light wavelength region. Therefore, they can also control radiant energy flow in this region. For all technologies mentioned above, the materials can be switched from one state to the other state by applying voltages. They all suffer from the drawback that they have only one function: either radiant energy-flow control or privacy control.

Here, we report liquid-crystal technology for switchable smart windows. It can be operated in dual mode to control both radiant energy flow and privacy. It contains a dichroic dye and LC dimers and exhibits both dielectric and flexoelectric effects. Liquid-crystal molecules usually have permanent dipoles, but they do not exhibit spontaneous polarization in a uniformly aligned state because of the equal probability for the dipoles to point in one direction and in the opposite direction. They are anisotropic dielectric media and their directions can be changed by externally applied electric fields under dielectric interactions. The dielectric interaction energy is given by

$$f_{\text{dielectric}} = -\frac{1}{2}\varepsilon_o \Delta\varepsilon (\vec{E}\cdot\vec{n})^2, \tag{1}$$

which is not sensitive to the polarity of the electric field, $\vec{E}$, where $\Delta\varepsilon$ is the dielectric anisotropy and $\vec{n}$ is the liquid-crystal director. However, if the liquid-crystal molecules do not have a perfect cylindrical shape, but are either bent or pear-shaped, when their orientation is not uniform in space, their dipoles may point in the same direction, and then a spontaneous polarization is produced and is given by [39–42]

$$\vec{P}_{\text{flexoelectric}} = e_s(\vec{n}\nabla\cdot\vec{n}) + e_b(\vec{n}\times\nabla\times\vec{n}), \tag{2}$$

where e_s and e_b are the splay and bent flexoelectric coefficients, respectively. Liquid crystals consisting of pear-shaped molecules are expected to have large splay flexoelectric coefficients. Liquid crystals consisting of bent molecules are expected to have large bent flexoelectric coefficients. The interaction of polarization and the externally applied electric field, $\vec{E}$, is described by [43,44]

$$f_{\text{flexoelectric}} = -\vec{P}_{\text{flexoelectric}}\cdot\vec{E} = -[e_s(\vec{n}\nabla\cdot\vec{n}) + e_b(\vec{n}\times\nabla\times\vec{n})]\vec{E}, \tag{3}$$

which is sensitive to the polarity of the applied electric field, namely, the polarity of the applied voltage. The orientation of the liquid crystal is determined by both the dielectric effect and the flexoelectric effect.

In this new smart window, when no voltage is applied, the LC material is in a uniform state and is transparent, and radiant energy can flow through, so that scenery behind the LC window can be seen. When a low-frequency voltage is applied, the LC is switched to a polydomain state under the influence of the flexoelectric effect. The LC window strongly scatters and weakly absorbs light. When a high-frequency voltage is applied, the LC is switched to a uniform absorbing state under the influence of the dielectric effect. The LC absorbs, but does not scatter, light.

II. OPERATION PRINCIPLES

In our newly designed LC window, the LC should have a small negative dielectric anisotropy ($\Delta\varepsilon < 0$) and a large flexoelectric coefficient. It is also doped with a small amount of a black dichroic dye. The mixture is filled in a cell with a homeotropic alignment. In the absence of an applied voltage, the LC is in the homeotropic state, as shown in Fig. 1(a), where the orientation of the LC is uniform and the material does not scatter light. Furthermore, the doped dye molecules are also in the homeotropic state and exhibit little absorption (the weak absorption is caused by the imperfect orientational ordering of the dye molecules due to thermal motion); therefore, the material is transparent. When a voltage is applied across the cell, the LC may reorient. The response of the LC depends on the frequency and amplitude of the applied voltage. Because the LC has nonzero dielectric anisotropy and flexoelectric coefficient, there are both dielectric and flexoelectric interactions. The dielectric interaction is insensitive to the polarity of the applied voltage, while the flexoelectric interaction is sensitive to the polarity of the applied voltage. When a low-frequency ac voltage is applied, the flexoelectric interaction is dominant in determining the reorientation of the LC, if the dielectric anisotropy is small and the flexoelectric coefficient is large. When a high-frequency ac voltage is applied, the flexoelectric interaction does not affect the reorientation of the LC because of the limited response speed of the LC.

We first consider the reorientation of the LC under a high-frequency voltage, where only the dielectric interaction is important. The electric field generated by the applied voltage is in the cell surface normal direction (the z direction): $\vec{E} = E\hat{z}$. The dielectric interaction energy is

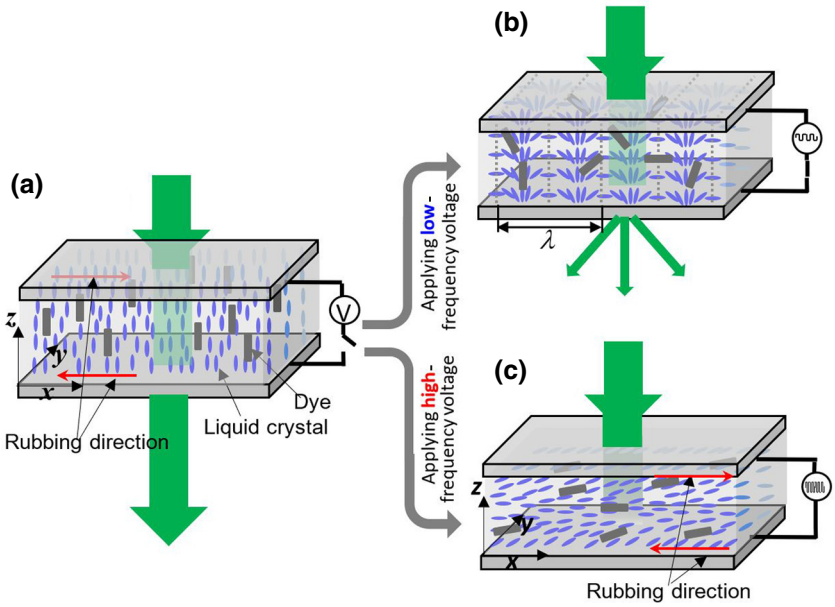

FIG. 1. Schematic diagram of the dual-mode smart window.

given by Eq. (1). The LC tends to align orthogonal to the electric field because of its negative dielectric anisotropy. When the LC reorients, its orientation will vary along the z direction because of the alignment layer. The nonuniform LC orientation produces an elastic energy, which disfavors reorientation. To induce reorientation of the LC, the applied voltage must be high enough that the decrease in the dielectric energy can compensate for the increase in the elastic energy. This electric-field-induced reorientation is known as a Fréedericksz transition and the threshold voltage for the transition is given by [45]

$$V_{\text{th}} = \pi\sqrt{K_{33}/\varepsilon_o|\Delta\varepsilon|}, \tag{4}$$

where K_{33} is the bent elastic constant. When a voltage higher than the threshold voltage (V_{th}) is applied, the LC is switched to the homogeneous state, as shown in Fig. 1(c), where the LC is parallel to the cell surface. The doped dye molecules become parallel to the cell substrate (in the x direction) and will absorb incident light with polarization in the x direction; therefore, the material becomes absorbing.

Now we consider reorientation of the LC under a low-frequency voltage. If the response time of the liquid crystal is τ, the frequency should be lower than $1/2\tau$. When the applied voltage is lower than V_{th}, the LC orientation is uniform and there is only dielectric interaction. When the applied voltage is higher than V_{th}, the LC orientation becomes nonuniform. A spontaneous electric polarization is induced and the flexoelectric interaction arises. The LC is switched to the striped state, as shown in Fig. 1(b). The flexoelectric interaction is much stronger than the dielectric interaction. We can neglect the dielectric interaction because of the small dielectric anisotropy. As an approximation, we also neglect the variation of the LC director in the z direction. The LC director is given by

$$n_x = \sin(kx), \quad n_y = 0, \quad n_z = \cos(kx), \tag{5}$$

where the wavevector is $k = 2\pi/\lambda$ and $\lambda/2$ is the width of the stripe. The induced electric polarization is given by

$$\begin{aligned}\vec{P}_{\text{flexoelectric}} &= e_s[\vec{n}(\nabla\cdot\vec{n})] + e_b[\vec{n}\times(\nabla\times\vec{n})] \\ &= e_s k\cos(kx)[\sin(kx)\hat{x} + \cos(kx)\hat{z}] \\ &\quad + e_b k\sin(kx)[-\cos(kx)\hat{x} + \sin(kx)\hat{z}],\end{aligned} \tag{6}$$

where e_s and e_b are the splay and bent flexoelectric coefficients, respectively. The flexoelectric interaction energy is given by

$$\begin{aligned}f_{\text{flexoelectric}} &= -\vec{E}\cdot\vec{P}_{\text{flexoelectric}} \\ &= -[e_s\cos^2(kx) + e_b\sin^2(kx)]Ek.\end{aligned} \tag{7}$$

The elastic energy is given by

$$\begin{aligned}f_{\text{elastic}} &= \frac{1}{2}K_{11}(\nabla\cdot\vec{n})^2 + \frac{1}{2}K_{33}(\vec{n}\times\nabla\times\vec{n})^2 \\ &= \frac{1}{2}k^2[K_{11}\cos^2(kx) + K_{33}\sin^2(kx)].\end{aligned} \tag{8}$$

The average (averaged over one stripe in the x direction) free energy density is

$$\begin{aligned}\bar{f} &= \langle f_{\text{elastic}} + f_{\text{flexoelectric}}\rangle \\ &= \frac{1}{4}k^2(K_{11}+K_{33}) - \frac{1}{2}(e_b+e_s)Ek.\end{aligned} \tag{9}$$

We minimize the average free energy density with respect to the wavevector k,

$$\frac{\partial \bar{f}}{\partial k} = \frac{1}{2}k(K_{11} + K_{33}) - \frac{1}{2}(e_b + e_s)E \overset{\text{let}}{=} 0.$$

to get

$$k = \frac{(e_b + e_s)E}{(K_{11} + K_{33})}. \tag{10}$$

The width of the stripe is

$$W = \frac{\lambda}{2} = \frac{\pi}{k} = \frac{\pi(K_{11} + K_{33})}{(e_b + e_s)E} = \frac{\pi(K_{11} + K_{33})d}{(e_b + e_s)V}, \tag{11}$$

where V is the applied voltage and d is the cell thickness. The width of the flexoelectric stripe is inversely proportional to the applied voltage V. The cell has a homeotropic alignment layer. There is no preferred direction for the stripes. Therefore, the stripes wiggle in the xy plane. Furthermore, when the applied voltage changes polarity, the LC director flips. Therefore, a polydomain structure is formed and the material becomes optically scattering.

III. EXPERIMENTAL RESULTS

To achieve a good performance, the liquid crystal should have the following properties: (1) a small negative dielectric anisotropy that can make the LC reorient to parallel to the cell substrate, when a voltage is applied, but does not suppress the flexoelectric effect, when a low-frequency voltage is applied, and (2) a large flexoelectric coefficient that can produce the flexoelectric stripe under a low voltage. After trial and error, we make a liquid-crystal mixture that has the desired properties. It consists of 10.0 wt % nematic liquid crystal, MAT978 (Merck); 64.0 wt % nematic liquid crystal, ZLI4330; 12.3 wt % liquid-crystal dimer, CB7CB; 12.2 wt % liquid-crystal dimer, CB9CB; and 1.5 wt % black dichroic dye. MAT978 has a dielectric anisotropy of −4.0. ZLI4330 has a dielectric anisotropy of −1.9. The dimers have a dielectric anisotropy of about +2.0 [46]. The dielectric anisotropy of the mixture is measured to be −0.3. Under dielectric interactions, the LC tends to align perpendicularly to externally applied electric fields. The dimers have bent molecular shapes and are known to exhibit large flexoelectric effects [47–51]. The LC is filled in cells assembled from two parallel glass plates with an ITO coating (electrode). The inner surfaces of the cells are coated with polyimide, SE1211 (Nissan Chemical), which generates a homeotropic alignment of the LC. The alignment layer is prebaked at 80 °C for 30 s, followed by a hard baking process at 180 °C for 1 h. It is also mechanically rubbed to generate a small (less than 1°) pretilt angle. The small pretilt angle can guide the initial rotation of the LC, but cannot control the direction of the flexoelectric stripe. The cell gap is controlled by 10 μm glass fibers.

We first study the response of the material to applied voltages under a polarizing optical microscope with crossed polarizers (Fig. 2). In the absence of an applied voltage, the LC is in the homeotropic state. The texture of the cell in the dark is shown in Fig. 2(a). When an ac voltage with a frequency of 1 kHz is applied, only the dielectric interaction plays a role in reorientation of the LC. The splay elastic constant, K_{11}, of ZLI4330 is 10 pN. We do not measure the elastic constant of the mixture. As an approximation, we use the elastic constant of ZLI4330. Using Eq. (4), the threshold voltage, V_{th}, is calculated to be 6.1 V. Experimentally, we find that the threshold voltage is 6.5 V. When the applied voltage is below 6.5 V, the state of the LC remains unchanged. When the applied voltage is increased above the threshold, the LC starts to tilt toward the direction parallel to the cell substrate. The LC exhibits optical retardation and rotates the polarization of the incident light, so the cell becomes brighter. The texture of the cell under 10 and 20 V is shown in Figs. 2(b) and 2(c), respectively. The texture is uniform and there is no light scattering. When an ac voltage with a frequency of 50 Hz is applied, the flexoelectric interaction dominates in reorienting the LC. When 10 V is applied, the LC is switched to the striped state, as shown in Fig. 2(d). The directions of the stripes are random and there is light scattering. When the applied voltage is increased, the width of the stripe decreases, as shown in Figs. 2(e)–2(g), and the scattering becomes stronger.

It is known that electroconvection can also induce a periodic striped structure (Williams domain) in liquid crystals with negative anisotropies, high ion density, and positive conductivity anisotropy [52–54]. The dimers used in our experiment are highly purified. We measure the resistivity of the LC used in our experiment and obtain a value of $3 \times 10^8\ \Omega \cdot \text{m}$ under a voltage of 1 V/1 kHz. The resistivity is high and it is unlikely to exhibit the electroconvection effect. Furthermore, in cells with homogeneous boundary conditions, the stripes induced through the electroconvection effect are usually perpendicular to the surface alignment direction; on the contrary, the stripe induced by flexoelectric effect is parallel to the alignment direction. To check whether the observed striped structure is induced by the flexoelectric effect or electroconvection effect, we make a liquid crystal consisting of 9.3 wt % nematic liquid crystal, MAT978 (Merck); 60.7 wt % nematic liquid crystal, ZLI4330; 15.0 wt % liquid-crystal dimer, CB7CB; and 15.0 wt % liquid-crystal dimer, CB9CB. This liquid crystal is filled in a cell with inner surfaces coated by the alignment material PI2170 (Nissan Chemicals), which is baked and rubbed for homogeneous alignment of the liquid crystals. The cell thickness is controlled by two micron spacers. Voltages of various amplitudes and frequencies are applied to the cell to study the striped structure. The

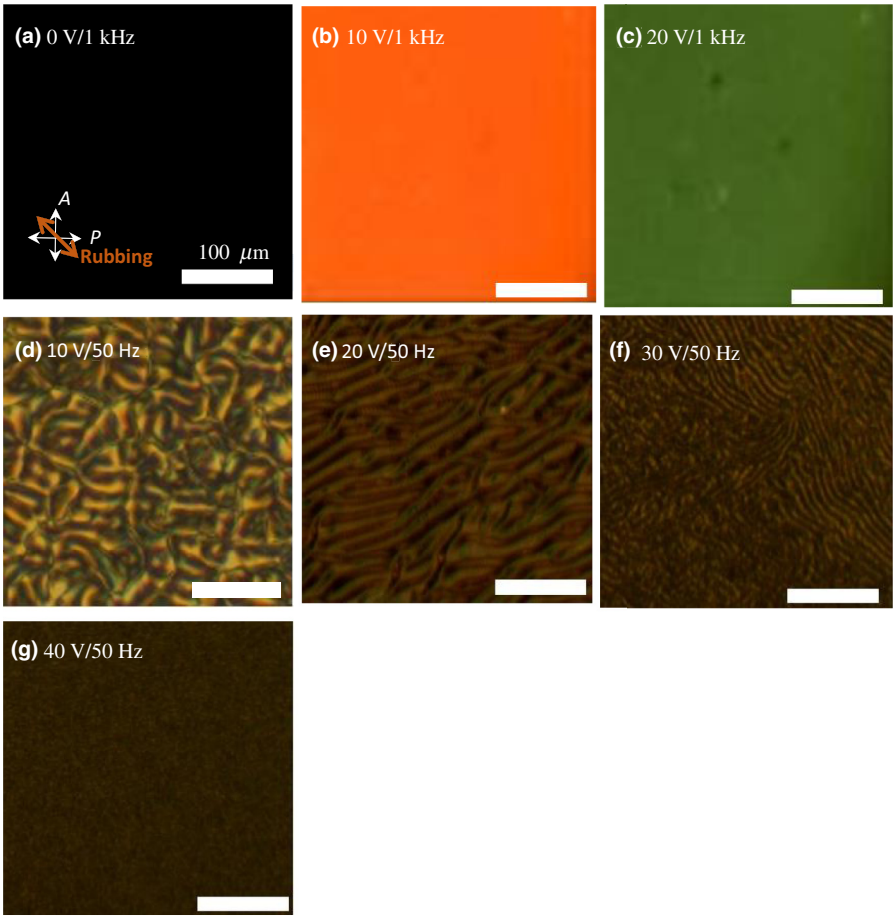

FIG. 2. Optical microphotographs of the LC cell with homeotropic alignment layer under various voltages and frequencies. Scale bars are 100 μm.

cell is studied under a polarizing optical microscope and the results are shown in Fig. 3. When no voltage is applied, the LC is in the homogeneous state. When the applied voltage is 5 V/0 Hz, the LC is switched to the striped state with the texture shown in Fig. 3(a). The stripes are in the same direction, parallel to the alignment layer rubbing direction, throughout the cell. When the applied voltage is increased, the periodicity decreases, but the direction of the stripes remains parallel to the alignment-layer rubbing direction, as shown in Figs. 3(b) and 3(c). When the applied voltage is 8 V/20 Hz, the striped structure is also observed, as shown in Fig. 3(d). When the frequency of the applied voltage is increased to 50 Hz, the directions of the stripes become more or less random. This result, that the stripe is parallel to the alignment direction under an applied voltage with low frequencies, indicates that the striped state in the cell is induced by the flexoelectric effect; this agrees with the results reported by Krishnamurthy *et al.* [53].

The scattering effect of the LC in the striped structure depends on the LC domain size, which is about the same as that of the width of the flexoelectric stripe. As shown by Eq. (11), the width of the stripe is controlled by the applied voltage. We measure the stripe widths at various applied voltages (Fig. 4). The width decreases with increasing applied voltage. The width versus the inversion of the applied voltage is approximately linear, which agrees well with the prediction by Eq. (11).

We then quantitatively measure the electro-optical response of the LC. In the measurements, a He–Ne green laser with a wavelength of 542 nm is used. The light is unpolarized and normally incident on the LC cell. The detector is a photodiode with a collection angle of 4°.

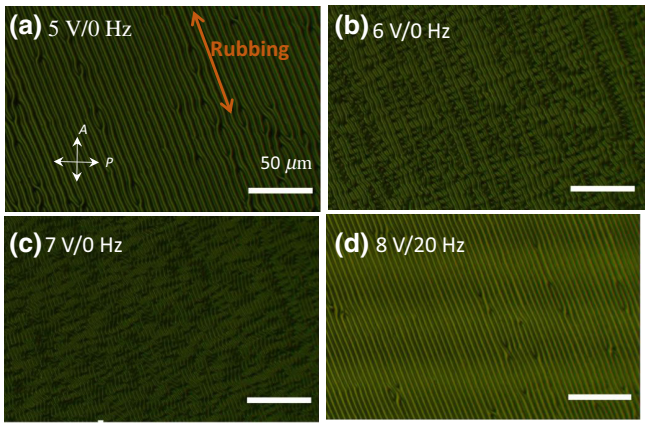

FIG. 3. Optical microphotographs of the LC cell with homogeneous alignment layer under various voltages and frequencies. Scale bars are 50 μm.

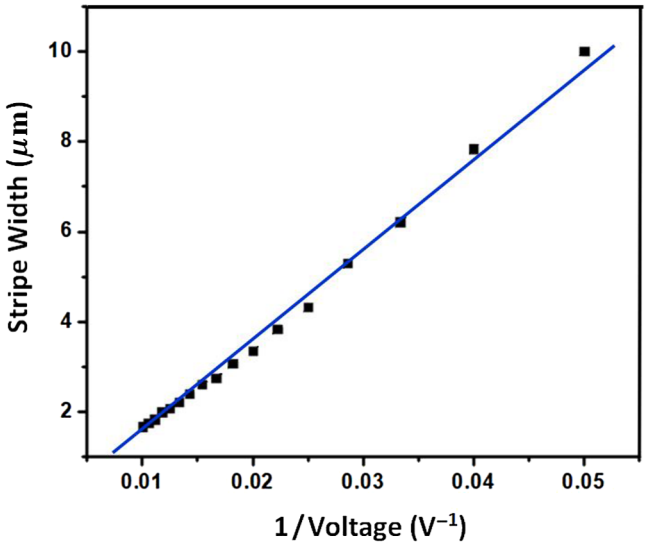

FIG. 4. Stripe width versus inversion of the applied voltage. The frequency of the applied voltage is 0 Hz. The line is a guide to the eye.

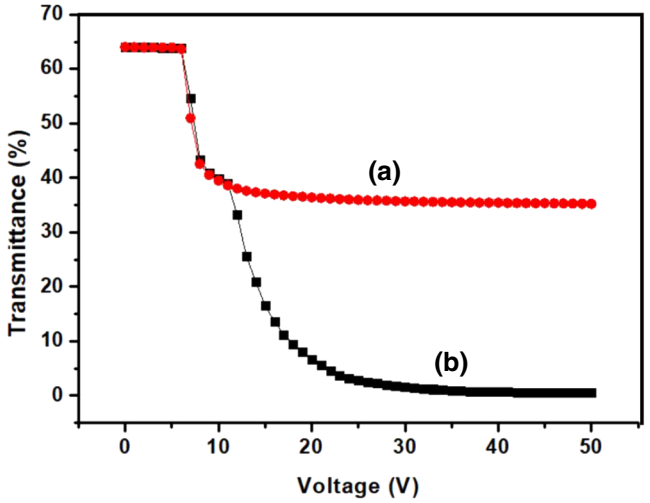

FIG. 5. Transmittance of the cell as a function applied voltage with two different frequencies: (a) 1 kHz and (b) 50 Hz. The wavelength of light used in measurements is 542 nm.

When the frequency of the applied voltage is 1 kHz, the result is shown by curve (a) in Fig. 5. Under this frequency, there is only a dielectric effect and no flexoelectric effect. There is no light scattering. The change in transmittance is due to the change of the absorption of the doped dye molecules. When the applied voltage is zero, the LC is in the homeotropic state and the transmittance is 65%. Light loss is caused by the residual absorption of the dye because the dye molecules are not exactly aligned along the cell normal direction due to thermal motion. When the applied voltage is increased above 6.5 V (the threshold voltage), the LC starts to tilt away from the cell normal and the material becomes more absorbing. Therefore, the transmittance begins to decrease. When the applied voltage is increased to 20 V, the transmittance reaches the minimum value of 36%. This minimum value is not very low because, when the LC molecules reorient, they are on the xz plane, as shown in Fig. 1(c), and only absorb incident light with polarization in the x direction. When the frequency of the applied voltage is 50 Hz, the result is shown by curve (b) in Fig. 5. For applied voltages below 10 V, the voltage dependence of the transmittance is the same as that when the frequency is 1 kHz because the LC director configuration is uniform and there are no flexoelectric stripes. When the applied voltage is increased above 10 V, the flexoelectric stripes begin to form and the material becomes scattering due to the flexoelectric interaction. The transmittance decreases more dramatically with increasing applied voltage. When the applied voltage is increased to 35 V, the transmittance reaches a minimum value of 0.5%. Notably, the low transmittance is due to some absorption caused by the dye molecules and scattering caused by the flexoelectric domains. Most of the scattered light is still in the forward direction [55].

The unpolarized incident light can be decomposed into two polarization components that are linearly polarized in two orthogonal directions. In the single-cell design discussed in the above paragraph, transmission modulation of the radiant energy-flow control mode (absorption mode) is small because the LC absorbs only one component of the incident light. To increase the modulation capability of transmittance of the absorption mode, we stack two LC cells with rubbing directions that are orthogonal to each other, such that both polarization components of the incident light are absorbed. The transmittance of the double cell as a function of applied voltage is shown in Fig. 6. In the voltage off state, the transmittance is 42%, which equals 0.65×0.65. When a voltage with 1 kHz frequency is applied, in one cell, the LC is rotated to the x direction to absorb the component of the incident light polarized in the x direction; in the other cell, the LC is rotated to the y direction to absorb the component of the incident light polarized in the y direction. The unpolarized incident light is absorbed more, as shown by curve (a) in Fig. 6. The minimum transmittance at 20 V becomes 3.8%. When the frequency of the applied voltage is changed to 50 Hz, the voltage dependence of the transmittance is shown by curve (b) in Fig. 6. The scattering of the double cell is also stronger than that in the single cell.

We also measure the transmission spectrum in the visible-light region of the LC cells under various applied voltages (Fig. 7). When no voltage is applied, the transmittance is high over the entire visible-light region, as shown by curve (b) in Fig. 7. When a voltage of 20 V/1 kHz is applied, the transmittance decreases significantly, as shown by curve (c) in Fig. 7, due to the absorption of the

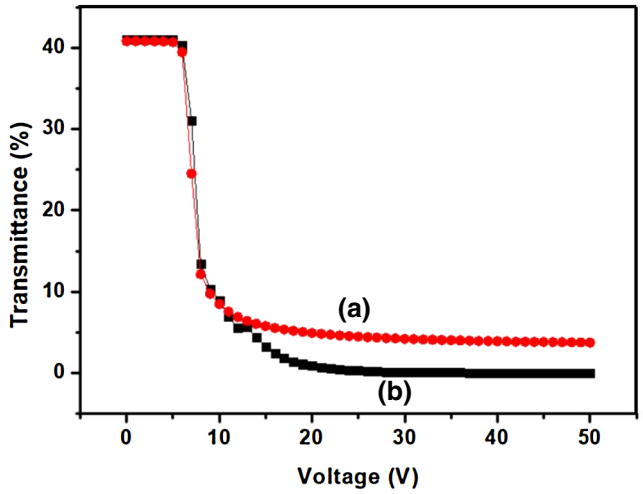

FIG. 6. Transmittance of the double cell as a function applied voltage with two different frequencies: (a) 1 kHz and (b) 50 Hz. The wavelength of light used in measurements is 542 nm.

dye. The spectra have a small dependence on the wavelength due to the wavelength-dependence absorption of the dichroic dye. The absorption of the dye becomes weaker for light with a wavelength longer than 650 nm. Above that wavelength, the transmittance increases with wavelength, as shown by curves (b) and (c) in Fig. 7. When a voltage of 40 V/50 Hz is applied, the transmittance becomes very low, as shown by curve (d) in Fig. 7. Scattering remains strong for light with a wavelength longer than 650 nm. Notably, when light is scattered, it is not absorbed, but deflected away from the original propagation direction.

Photographs of the (double cell) dual-mode switchable window are shown in Fig. 8. A Kent State University logo is placed behind the window. The distance between the

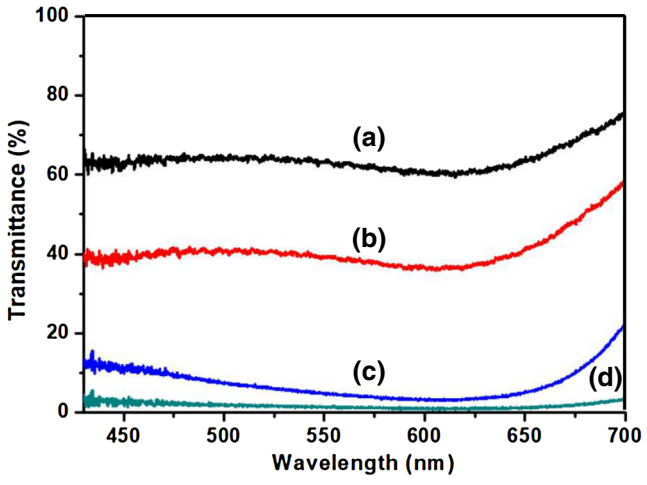

FIG. 7. Transmission spectra of the cells under various applied voltages: (a) a single cell at 0 V, (b) a double cell at 0 V, (c) a double cell at 20 V/1 kHz, and (d) a double cell at 40 V/50 Hz.

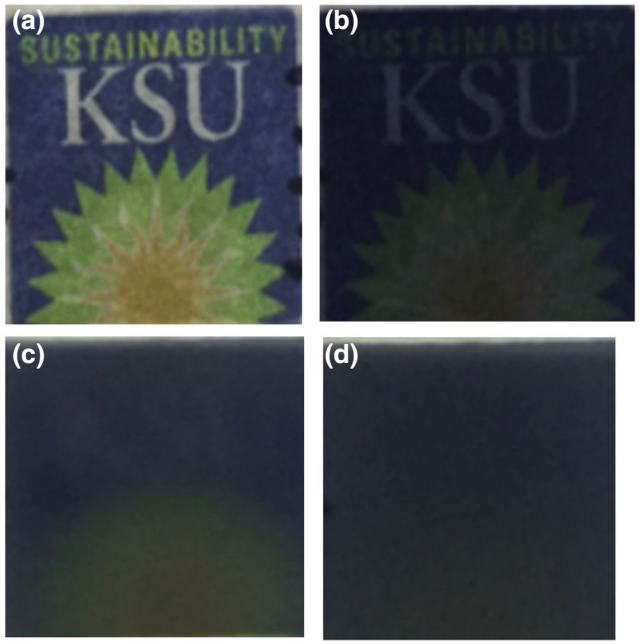

FIG. 8. Photographs of the dual-mode double-cell liquid-crystal switchable window under various applied voltages: (a) 0 V, (b) 20 V/1 kHz, (c) 20 V/50 Hz, and (d) 40 V/50 Hz.

logo and the LC layer is about 5 mm. When no voltage is applied, the window is transparent with high transmittance and without haze, as shown in Fig. 8(a), so the logo can be seen. When a voltage of 20 V with a frequency of 1 kHz is applied, the transmittance of the window decreases, but the haze remains low, as shown in Fig. 8(b). The image of the logo is not distorted, and thus, can still be seen. When a voltage of 20 V with a frequency of 50 Hz is applied, the window becomes opaque, as shown in Fig. 8(c) so the image of the logo is frosted. When the voltage is increased to 40 V, scattering is increased and the logo cannot be seen, as shown in Fig. 8(d).

IV. CONCLUSION

We develop a dual-mode switchable liquid-crystal window that can control both radiant energy flow and privacy. The modes are selected by using different voltage frequencies. A dichroic dye is doped to enable modulation of transmission of the window. In the absence of an applied voltage, the window is transparent without haze. When a high-frequency (1 kHz) voltage is applied, the LC and doped dye molecules inside the window reorient uniformly under dielectric interactions. The material becomes optically absorbing. The transmittance decreases, but the haze does not change. In this mode, the window can control radiant energy flow through the window. When a low-frequency (50 Hz) voltage is applied, the LC and doped dye molecules are switched into a micron-sized polydomain structure under flexoelectric interactions. The

material becomes optically scattering and absorbing. The scenery behind the window is blocked. In this mode, privacy can be controlled. This dual-mode switchable window is suitable for architectural and automobile windows.

[1] R. Baetens, B. P. Jelle, and A. Gustavsen, Properties, requirements and possibilities of smart windows for dynamic daylight and solar energy control in buildings: A state-of-the-art review, Sol. Energy Mater. Sol. Cells **94**, 87 (2010).

[2] D. Ge, E. Lee, L. Yang, Y. Cho, M. Li, D. S. Gianola, and S. Yang, A robust smart window: Reversibly switching from high transparency to angle-independent structural color display, Adv. Mater. **27**, 2489 (2015).

[3] E. Syrrakou, S. Papaefthimiou, and P. Yianoulis, Eco-efficiency evaluation of a smart window prototype, Sci. Total Environ. **359**, 267 (2006).

[4] A. Cocchia, in *Smart city* (Springer, Cham, 2014), pp. 13–43.

[5] C. Xu, L. Liu, S. E. Legenski, D. Ning, and M. Taya, Switchable window based on electrochromic polymers, J. Mater. Res. **19**, 2072 (2004).

[6] A. Ghosh, B. Norton, and A. Duffy, Measured overall heat transfer coefficient of a suspended particle device switchable glazing, Appl. Energy **159**, 362 (2015).

[7] K. Wang, H. Wu, Y. Meng, Y. Zhang, and Z. Wei, Integrated energy storage and electrochromic function in one flexible device: An energy storage smart window, Energy Environ. Sci. **5**, 8384 (2012).

[8] A. Azens and C. Granqvist, Electrochromic smart windows: Energy efficiency and device aspects, J. Solid State Electrochem. **7**, 64 (2003).

[9] C. G. Granqvist, A. Azens, J. Isidorsson, M. Kharrazi, L. Kullman, T. Lindström, G. A. Niklasson, C.-G. Ribbing, D. Rönnow, M. S. Mattsson, and M. Veszelei, Towards the smart window: Progress in electrochromics, J. Non. Cryst. Solids **218**, 273 (1997).

[10] D.-K. Yang and S.-T. Wu, *Fundamentals of Liquid Crystal Devices* (John Wiley & Sons, New York, 2014).

[11] P. S. Drzaic, *Liquid Crystal Dispersions* (World Scientific, NJ, 1995).

[12] J. W. Doane, N. A. Vaz, B.-G. Wu, and S. Zumer, Field controlled light scattering from nematic microdroplets, Appl. Phys. Lett. **48**, 269 (1996).

[13] D. Cupelli, F. P. Nicoletta, S. Manfredi, M. Vivacqua, P. Formoso, G. D. Filpo, and G. Chidichimo, Self-adjusting smart windows based on polymer-dispersed liquid crystals, Sol. Energy Mater. Sol. Cells **93**, 2008 (2009).

[14] J. Erdmann, J. W. Doane, S. Zumer, and G. Chidichimo, in *Liquid Crystal Chemistry, Physics, and Applications*, Vol. 1080 (Int. Soc. Opt. Photonics, 1989), p. 32.

[15] B. Wu, J. H. Erdmann, and J. W. Doane, Response times and voltages for PDLC light shutters, Liq. Cryst. **5**, 1453 (1989).

[16] J. Kelly, W. Wu, and P. P. Muhoray, Wavelength dependence of scattering in PDLC films: Droplet size effects, Mol. Cryst. Liq. Cryst. Sci. Technol., Sect. A **223**, 251 (1992).

[17] W. Korner, H. Scheller, A. Beck, and J. Fricke, PDLC films for control of light transmission, J. Phys. D: Appl. Phys. **27**, 2145 (1994).

[18] D.-K. Yang, L.-C. Chien, and J. W. Doane, Cholesteric liquid crystal/polymer dispersion for haze-free light shutters, Appl. Phys. Lett. **60**, 3102 (1992).

[19] J. Ma, L. Shi, and D.-K. Yang, Bistable polymer stabilized cholesteric texture light shutter, Appl. Phys. Express **3**, 021702 (2010).

[20] D.-K. Yang, L. C. Chien, and J. W. Doane, in *Display Research Conference, Conference Record of the 1991 International* (1991), p. 49.

[21] R. Bao, C.-M. Liu, and D.-K. Yang, Smart bistable polymer stabilized cholesteric texture light shutter, Appl. Phys. Express **2**, 112401 (2009).

[22] F. Ahmad, M. Jamil, and Y. J. Jeon, Reverse mode polymer stabilized cholesteric texture (PSCT) light shutter display–A short review, J. Mol. Liq. **233**, 187 (2017).

[23] R. Ma and D.-K. Yang, Polymer-stabilized cholesteric-texture reverse-mode light shutter: Cell design, J. Soc. Inf. Display **6**, 125 (1998).

[24] D.-K. Yang, X.-Y. Huang, and Y.-M. Zhu, Bistable cholesteric reflective displays: Materials and drive schemes, Annu. Rev. Mater. Sci. **27**, 117 (1997).

[25] M. Xu and D.-K. Yang, Dual frequency cholesteric light shutters, Appl. Phys. Lett. **70**, 720 (1997).

[26] A. Moheghi, H. Nemati, Y. Li, Q. Li, and D.-K. Yang, Bistable salt doped cholesteric liquid crystals light shutter, Opt. Mater. **52**, 219 (2016).

[27] S.-T. Wu and D.-K. Yang, *Reflective Liquid Crystal Displays* (Wiley, New York, 2001).

[28] D.-K. Yang, J. W. Doane, Z. Yaniv, and J. Glasser, Cholesteric reflective display: Drive scheme and contrast, Appl. Phys. Lett. **64**, 1905 (1994).

[29] M. Xu, F. Xu, and D.-K. Yang, Effects of cell structure on the reflection of cholesteric liquid crystal displays, J. Appl. Phys. **83**, 1938 (1998).

[30] C.-W. Chen, A. N. Brigeman, T.-J. Ho, and I. C. Khoo, Normally transparent smart window based on electrically induced instability in dielectrically negative cholesteric liquid crystal, Opt. Mater. Express **8**, 691 (2018).

[31] D. J. Broer, J. Lub, and G. N. Mol, Wide-band reflective polarizers from cholesteric polymer networks with a pitch gradient, Nature **378**, 467 (1995).

[32] L. Li and S. M. Faris, A single-layer super broadband reflective polarizer, SID Tech. Digest **37**, 111 (1996).

[33] M. Mitov, Cholesteric liquid crystals with a broad light reflection band, Adv. Mater. **24**, 6260 (2012).

[34] C. Binet, M. Mitov, and M. Mauzac, Switchable broadband light reflection in polymer-stabilized cholesteric liquid crystals, J. Appl. Phys. **90**, 1730 (2001).

[35] S.-W. Oh, S. Kim, J. Baek, and T. Yoon, Optical and thermal switching of liquid crystals for self-shading windows, Adv. Sustainable Syst. **2**, 1700164 (2018).

[36] B. Yu, J. Huh, K. Kim, and T. Yoon, Light shutter using dichroic-dye-doped long-pitch cholesteric liquid crystals, Opt. Express **21**, 29332 (2013).

[37] S. Kim, S. Oh, and T. Yoon, Enhancement of absorption and haze with hybrid anchoring of dye-doped cholesteric liquid crystals, Opt. Express **26**, 14259 (2018).

[38] S. Oh, J. Baek, J. Heo, and T. Yoon, Dye-doped cholesteric liquid crystal light shutter with a polymer-dispersed liquid crystal film, Dyes Pigm. **134**, 36 (2016).
[39] R. B. Meyer, Piezoelectric Effects in Liquid Crystals, Phys. Rev. Lett. **22**, 918 (1969).
[40] Y. Jiang, X. Zhou, G. Qin, X. Xu, S. Lee, and D.-K. Yang, Effects of flexoelectricity and ion on the flicker of fringe field switching liquid crystal display, SID Symp. Dig. Tech. Pap. **49**, 1095 (2018).
[41] J. S. Patel and R. B. Meyer, Flexoelectric Electro-Optics of a Cholesteric Liquid Crystal, Phys. Rev. Lett. **58**, 1538 (1987).
[42] J. Harden, B. Mbanga, N. Éber, K. F. Csorba, S. Sprunt, J. T. Gleeson, and Antal Jakli, Giant Flexoelectricity of Bent-Core Nematic Liquid Crystals, Phys. Rev. Lett. **97**, 157802 (2006).
[43] Y. P. Bobylev, V. G. Chigrinov, and S. A. Pikin, Threshold flexoelectric effect in nematic liquid crystal, J. Phys. Colloques **40**, C3 (1979).
[44] A. J. Davidson and N. J. Mottram, Flexoelectric switching in a bistable nematic device, Phys. Rev. E **65**, 051710 (2002).
[45] P. G. de Gennes and J. Prost, *The Physics of Liquid Crystals* (Oxford University Press, New York, 1993).
[46] G. Babakhanova, Z. Parsouzi, S. Paladugu, H. Wang, Y. A. Nastishin, S. V. Shiyanovskii, S. Sprunt, and O. D. Lavrentovich, Elastic and viscous properties of the nematic dimer CB7CB, Phys. Rev. E **96**, 062704 (2017).
[47] X. Zhou, Y. Jiang, G. Qin, X. Xu, and D.-K. Yang, Static and Dynamic Properties of Hybridly Aligned Flexoelectric in-Plane-Switching Liquid-Crystal Display, Phys. Rev. Appl. **8**, 054033 (2017).
[48] Y. Jiang, X. Zhou, Y. Shin, G. Qin, X. Xu, L. Zhou, S. Lee, and D.-K. Yang, Image flickering reduction by dimer and polymer stabilization in FFS liquid crystal display, J. Soc. Inf. Display **27**, 285 (2019).
[49] A. Varanytsia and L.-C. Chien, Giant flexoelectro-optic effect with liquid crystal dimer CB7CB, Sci. Rep. **7**, 41333 (2017).
[50] J. A. Fells, X. Wang, S. J. Elston, C. Welch, G. H. Mehl, M. J. Booth, and S. M. Morris, Flexoelectro-optic liquid crystal analog phase-only modulator with a 2π range and 1 kHz switching, Opt. Lett. **43**, 4362 (2018).
[51] V. Joshi, K. Chang, A. Varanytsia, D. A. Paterson, J. M. Storey, C. T. Imrie, and L.-C. Chien, Cholesteric metronomes with flexoelectrically programmable amplitude, Adv. Opt. Mater. **6**, 1800013 (2018).
[52] G. Pucci, F. Carbone, G. Lombardo, C. Versace, and R. Barberi, Topologically non-equivalent textures generated by the nematic electrohydrodynamics, Liq. Cryst. **46**, 649 (2018).
[53] K. S. Krishnamurthy, N. B. Palakurthy, and C. V. Yelamaggad, Confined electroconvective and flexoelectric instabilities deep in the freedericksz state of nematic CB7CB, J. Phys. Chem. B **121**, 5447 (2017).
[54] N. Éber, P. Salamon, and Á Buka, Electrically induced patterns in nematics and how to avoid them, Liq. Cryst. Rev. **4**, 101 (2016).
[55] P. Nolan, M. Tillin, D. Coates, E. Ginter, E. Lueder, and T. Kallfass, Reflective mode PDLC displays-paper white display, Proc. EuroDisplay **93**, 397 (1993).